Muñoz Portero, MJ.; García Antón, J.; Guiñón Segura, JL.; Leiva García, R. (2011). Pourbaix diagrams for titanium in concentrated aqueous lithium bromide solutions at 25 ºC. Corrosion Science. 53(4):1440-1450. doi:10.1016/j.corsci.2011.01.013.

# Pourbaix diagrams for titanium in concentrated aqueous lithium bromide solutions at 25 ºC

M.J. Muñoz-Portero, J. García-Antón*, J.L. Guiñón, R. Leiva-García

*Departamento de Ingeniería Química y Nuclear. Universidad Politécnica de Valencia*

*P.O. Box 22012, E-46071 Valencia (Spain)*

**ABSTRACT**

Pourbaix diagrams (electrode potential-pH diagrams) for Ti-$Br^-$-$H_2O$ system at 25 ºC in the absence and presence of titanium hydrides were developed in 400 g/L, 700 g/L, 850 g/L, and 992 g/L LiBr solutions. The diagrams were compared with the simple Ti-$H_2O$ system at 25 ºC. Comparison of the simple Ti-$H_2O$ system with the diagrams of the Ti-$Br^-$-$H_2O$ system at 25 ºC showed that the titanium solubility range in the acid, neutral, and weak alkaline areas of the diagrams extended slightly to both higher pH values and potentials with increasing bromide ion activity and decreasing water activity.

*Keywords*:

A. Titanium.

A. Lithium bromide.

C. Activity.

C. Pourbaix diagram.

* Corresponding author. Phone: +34963877632; Fax: +34963877639.

E-mail address: jgarciaa@iqn.upv.es (J. Garcia-Antón)

## 1. Introduction

Aqueous solutions containing high concentrations of lithium bromide (LiBr) are typical absorbent solutions in heating and refrigerating absorption systems that use natural gas or steam as energy sources [1-6]. Although LiBr possesses favourable thermophysical properties, it can cause serious corrosion problems on metallic components in refrigeration systems and heat exchangers in absorption plants [7-36].

With the advances in refrigeration technology new double effect LiBr absorption systems have been developed. These systems exhibit a higher energetic efficiency than single effect machines, although they also reach higher temperatures, which may cause important corrosion problems. Titanium is used in heat exchangers as it possesses good thermal, mechanical, and corrosion resistance properties. The high corrosion resistance of titanium is due to the formation of a stable, adherent, tenacious, and permanent oxide film on its surface. This film protects titanium and gives it its excellent resistance to corrosion in a wide range of aggressive media, such as halide solutions. That is why titanium can be employed in LiBr absorption refrigeration systems. Despite this, few studies have been found in the literature that analyze titanium corrosion resistance in highly concentrated LiBr solutions [8,13,15,26,30].

One of the most relevant problems that corrosion can cause in these systems is the generation of hydrogen as a consequence of the electrochemical phenomenon. The generation of hydrogen causes significant efficiency losses due to the presence of non-condensable gases since theses machines work under vacuum conditions. The effect of

non-condensable gases on the performance of absorbers has been studied previously [37,38]. They reported that the evolution of hydrogen in the LiBr/water absorber reduces its absorption performance, reducing the absorption system's overall coefficient of performance (COP). Some previous corrosion studies on several materials have determined that hydrogen increases the anodic current density, and decreases the stability of passive film and hinder the repassivation process [31,39,40].

Chemical and electrochemical equilibria data are commonly represented in Pourbaix diagrams, which are electrode potential-pH diagrams. Pourbaix diagrams have been extensively used to predict and analyze corrosion-related processes. The diagrams indicate the potential and pH conditions under which the metal is stable thermodynamically (or immune to corrosion) and the conditions that may cause the dissolution of the metal in the form of ions (corrosion) or its transformation into metal oxides, hydroxides, hydrides or salts and further passivation [41-47].

Pourbaix diagrams for copper [48], nickel [49], and chromium [50] in concentrated aqueous LiBr solutions at 25 ºC have been reported in previous works, which are particularly useful to study the corrosion behaviour of these metals and its alloys in refrigeration systems.

The goal of the present work was the analysis of the general conditions of immunity, passivation, and corrosion for titanium in concentrated aqueous LiBr solutions in the absence and presence of titanium hydrides, which have not been reported in the literature. Pourbaix diagrams (electrode potential-pH diagrams) for Ti-

$Br^-$-$H_2O$ system at 25 ºC were developed in 400 g/L, 700 g/L, 850 g/L, and 992 g/L (4.61 M, 8.06 M, 9.79 M, and 11.42 M) LiBr solutions, which are common concentrations in different parts of absorption devices. The diagrams were compared with the simple Ti-$H_2O$ system at 25 ºC.

## 2. Procedure

### *2.1. Standard Gibbs free energies of formation*

Pourbaix diagrams were constructed from standard Gibbs free energy of formation ($\Delta G_f^o$) data at 25 ºC for all the species considered. Twelve chemical species were considered for the Ti-$H_2O$ system:

1. Seven solid species: Ti, TiO, $Ti_2O_3$, $Ti(OH)_3$, $Ti_3O_5$, $TiO_2$, and $TiO_2 \cdot H_2O$.
2. Five aqueous species: $Ti^{+2}$, $Ti^{+3}$, $TiO^{+2}$, $HTiO_3^-$, and $TiO_2^{+2}$.

For the construction of the Pourbaix diagrams for the Ti-$Br^-$-$H_2O$ system, three additional solid species were considered, as well as the twelve species of the Ti-$H_2O$ system. These solid species are: $TiBr_2$, $TiBr_3$, and $TiBr_4$.

For the construction of the Pourbaix diagrams in the presence of titanium hydrides, two additional solid species were considered: $TiH_2$ and TiH. Therefore, the total number of species was fourteen for the Ti-$H_2O$ system and seventeen for the Ti-$Br^-$-$H_2O$ system. Pourbaix diagrams for titanium in concentrated aqueous LiBr solutions

considering the titanium hydrides can be useful to study the corrosion behaviour of titanium in the presence of hydrogen in the absorption plants.

The $\Delta G_f^o$ values used to calculate the equilibria are listed in Table 1, together with the oxidation number, and the state of the species. The thermodynamic data for all the species are those selected by Bard et al. [51].

*2.2. Reactions*

Equations of different reactions were written between all species in the Ti-$Br^-$-$H_2O$ system. Pairs of species (A and B) were considered in each reaction together with the $H^+$ ion, the electrical charge ($e^-$), $H_2O$, and the $Br^-$ ion. The reaction equations had the following general form:

$$a\,A + m\,H^+ + n\,e^- \rightleftarrows b\,B + c\,H_2O + d\,Br^- \qquad (1)$$

where A and B are the two species containing titanium involved in the reaction.

The reaction equations used for the construction of the Pourbaix diagrams for the Ti-$Br^-$-$H_2O$ system are shown in Tables 2-5. The reactions used for the simple Ti-$H_2O$ system are shaded.

For the Ti-$H_2O$ system, twelve species were considered with a total number of reactions of 66. For the Ti-$Br^-$-$H_2O$ system, fifteen species were considered with a total number of reactions of 105. Reactions were divided into four types:

1. *Electrochemical reactions involving* $H^+$. These electrochemical reactions depended both on the potential and the pH; they were represented by *oblique lines* in a Pourbaix diagram. The number of reactions was 50 for the Ti-$H_2O$ system and 70 for the Ti-$Br^-$-$H_2O$ system (Table 2).
2. *Electrochemical reactions not involving* $H^+$. These electrochemical reactions were dependent on the potential and independent of the pH; they were represented by *horizontal lines* in a Pourbaix diagram. The number of reactions was 6 for the Ti-$H_2O$ system and 16 for the Ti-$Br^-$-$H_2O$ system (Table 3).
3. *Chemical reactions involving* $H^+$. These chemical reactions were independent of the potential and dependent on the pH; they were represented by *vertical lines* in a Pourbaix diagram. The number of reactions was 8 for the Ti-$H_2O$ system and 15 for the Ti-$Br^-$-$H_2O$ system (Table 4).
4. *Chemical reactions not involving* $H^+$. These chemical reactions were independent both of the potential and the pH; they were not represented in a Pourbaix diagram, but they were used for the calculation of the equilibrium conditions. The number of reactions was 2 for the Ti-$H_2O$ system and 4 for the Ti-$Br^-$-$H_2O$ system (Table 5).

The reactions were classified as: 1) homogeneous reactions (involving all the dissolved species), 2) heterogeneous reactions with two solid species, and 3) heterogeneous reactions with one solid species.

In the presence of titanium hydrides, additional electrochemical reactions involving $H^+$ were considered: 25 reactions for the Ti-$H_2O$ system and 31 reactions for the Ti-$Br^-$-$H_2O$ system, as shown in Table 6. For the Ti-$H_2O$ system in the presence of titanium hydrides, fourteen species were considered and the total number of reactions increased from 66 to 91. Seventeen species were considered for the Ti-$Br^-$-$H_2O$ system in the presence of titanium hydrides, so that the total number of reactions increased from 105 to 136.

Conventional procedures were used to calculate the electrochemical and chemical equilibria from $\Delta G_f^o$ data [41].

## 3. Results

Equilibria for the Ti-$Br^-$-$H_2O$ system at 25 ºC were determined for activities of bromide species representative of the test solutions. The values of the $Br^-$ ion activity were 15.61, 194.77, 650.06, and 2,042.65, which corresponded to the 400 g/L, 700 g/L, 850 g/L, and 992 g/L (4.61 M, 8.06 M, 9.79 M, and 11.42 M) LiBr solutions, respectively. These extremely high activity values are due to the very large activity coefficients of the LiBr solutions. The calculation of the activity values of strong electrolytes in aqueous solutions has generally been difficult because of the lack of

activity coefficient data. The Debye-Hückel equation unfortunately applies only to dilute solutions with concentrations far below those used in industrials applications. Meissner and Kusik developed a model to calculate the activity coefficients of strong electrolyte in aqueous solutions [52,53], which was described in detail in a previous work [48]. The activity coefficients of 400 g/L, 700 g/L, 850 g/L, and 992 g/L aqueous LiBr solutions were 2.973, 19.095, 49.472, and 124.78, respectively.

Activities of the $Br^-$ ion were obtained by converting the molar concentrations of 4.61 M, 8.06 M, 9.79 M, and 11.42 M to their corresponding molal concentrations of 5.25 m, 10.20 m, 13.14 m, and 16.37 m, and using molality-dependent activity coefficients. The densities of the 400 g/L, 700 g/L, 850 g/L, and 992 g/L LiBr solutions used for converting molarity to molality were 1.2766 g/cm$^3$, 1.4904 g/cm$^3$, 1.5948 g/cm$^3$, and 1.6896 g/cm$^3$, respectively, which were calculated using the correlation proposed by Patterson and Pérez-Blanco [54].

The activity values of water in 400 g/L, 700 g/L, 850 g/L, and 992 g/L LiBr solutions were 0.715, 0.358, 0.216, and 0.118, respectively, according to the method proposed by Meissner and Kusik [53,55], and described in detail in previous works [49,50]. The activity values of water in 400 g/L, 700 g/L, 850 g/L, and 992 g/L LiBr solutions were obtained using ionic strengths of 5.25, 10.20, 13.14, and 16.37, and reduced activity coefficients of the pure solution at 25 ºC of 2.973, 19.095, 49.472, and 124.78, respectively. The activities of the dissolved species containing titanium were plotted for $10^{-6}$, $10^{-4}$, $10^{-2}$, and $10^{0}$.

Fig. 1 shows the Pourbaix diagram of the Ti-$H_2O$ system at 25 ºC. The Pourbaix diagrams of the Ti-$Br^-$-$H_2O$ system at 25 ºC for $Br^-$ activities of 15.61, 194.77, 650.06, and 2,042.65, and water activities of 0.715, 0.358, 0.216, and 0.118 are presented in Fig. 2-5, respectively. Fig. 1a-5a show the Pourbaix diagrams not considering the titanium hydrides and Fig. 1b-5b show the Pourbaix diagrams considering the titanium hydrides, which can be useful to study the corrosion behaviour of titanium in the presence of hydrogen in the absorption plants. Solid lines delimit the stability regions of the solid phases in equilibrium with $10^{-6}$, $10^{-4}$, $10^{-2}$, and $10^{0}$ activity values of the soluble titanium species. Fine broken lines show equilibria between the dissolved species. In this work the Pourbaix diagrams and predominance diagrams of the dissolved species were superimposed to show the predominating dissolved species in each part of the solid stability areas in the Pourbaix diagrams.

Simplified Pourbaix diagrams for titanium in $H_2O$ at 25 ºC are shown in Fig. 6 and 7 not considering and considering the titanium hydrides, respectively, in the absence of $Br^-$ ion (Fig. 6a and 7a), for a $Br^-$ activity of 15.61 (Fig. 6b and 7b), for a $Br^-$ activity of 194.77 (Fig. 6c and 7c), for a $Br^-$ activity of 650.06 (Fig. 6d and 7d), and for a $Br^-$ activity of 2,042.65 (Fig. 6e and 7e). These diagrams were plotted for a $10^{-6}$ activity of the soluble titanium species, which was used to separate between corrosion, immunity, and passivation. The corrosion areas were shaded to differentiate them from immunity and passivation.

Coarse broken lines in Fig. 1-7, labelled “a” and “b”, delimit the stability area of $H_2O$ at a partial pressure of the gaseous species equal to 1 atm. The upper line (a)

represents the oxygen equilibrium line ($O_2(g)/H_2O(l)$), and potentials above this line will oxidize $H_2O$ as oxygen forms. The lower line (b) represents the hydrogen equilibrium line ($H^+(aq)/H_2(g)$), and potentials below this line will result in hydrogen formation. The potential values reported in this work are always related to the standard hydrogen electrode (SHE), which is considered to be zero at 25 ºC. All the diagrams in Fig. 1-7 were drawn using Autocad.

The thermodynamic stability of the titanium species in the Ti-$Br^-$-$H_2O$ system is summarized in Table 7, where "a" stands for stability in the Pourbaix diagram not considering the titanium hydrides, and "b" stands for stability in the Pourbaix diagram considering the titanium hydrides. Unmarked species do not appear in the diagrams at any $Br^-$ activity at the activity values of the soluble titanium species used.

It notes that the Pourbaix diagrams for titanium in concentrated aqueous LiBr solutions of 400 g/L, 700 g/L, 850 g/L, and 992 g/L at 25 ºC have not been reported in the literature, and are original in this work.

## 4. Discussion

### *4.1. Pourbaix diagrams for titanium in concentrated aqueous LiBr solutions not considering the titanium hydrides*

The Pourbaix diagram of the simple Ti-$H_2O$ system at 25 ºC (Fig. 1a) shows that titanium is a very reactive metal, as the immunity region is situated below the hydrogen

equilibrium line ($H^+(aq)/H_2(g)$). Titanium corrodes in acid, neutral, and weak alkaline solutions to form $Ti^{+2}$. An increase in $Ti^{+2}$ activity from $10^{-6}$ to $10^0$ results in a higher potential value for the formation of $Ti^{+2}$ from titanium. $Ti^{+2}$ can form TiO. An increase in $Ti^{+2}$ activity from $10^{-6}$ to $10^0$ results in a lower pH value for the formation of TiO from $Ti^{+2}$. Alkaline solutions passivate titanium by the formation of TiO. Ti (II) species ($Ti^{+2}$ or TiO) can oxidize further to three, four, or six valent forms. Depending on pH and activity of the dissolved titanium species, Ti (III) species can be either an aqueous species ($Ti^{+3}$), which involves corrosion, or a solid compound ($Ti_2O_3$), which involves passivation. An increase in the activity of $Ti^{+2}$ from $10^{-6}$ to $10^0$ results in an decrease of electrochemical potential for a given pH value at which there is equilibrium between $Ti_2O_3$ and $Ti^{+2}$. Ti (III) species ($Ti^{+3}$ and $Ti_2O_3$) and $Ti^{+2}$ can oxidize to form a solid Ti (IV) species ($TiO_2$), which forms a wide passivation area. At very high potentials, $TiO_2$ oxidizes to form an aqueous Ti (VI) species ($TiO_2^{+2}$), which creates a corrosion area at all pH-values. An increase in the activity of $TiO_2^{+2}$ from $10^{-6}$ to $10^0$ results in an increase of the electrochemical potential at which there is equilibrium between $TiO_2$ and $TiO_2^{+2}$. It can be concluded that the activity of the dissolved titanium species changes the dimension of the different stability areas of immunity, passivation, and corrosion. The immunity area (stability of the metal) and the passivation area (stability of solid compounds) increase by increasing the activity of the dissolved titanium species. The corrosion area (stability of the dissolved species) at acid, neutral, and weak alkaline pH, and the pH-independent corrosion area at high potentials decrease by increasing the activity of the dissolved titanium species.

Comparison of the diagram of the simple Ti-$H_2O$ system at 25 ºC in Fig. 1a with the diagrams of the Ti-$Br^-$-$H_2O$ system at 25 ºC in Fig. 2a-5a shows that the titanium solubility range in the acid, neutral, and weak alkaline areas of the diagrams extends slightly to both higher pH values and potentials with increasing bromide ion activity and decreasing water activity, as a result of destabilization of the solid species TiO, $Ti_2O_3$, and $TiO_2$.

The precipitation of TiO is governed by the chemical equilibrium with $Ti^{+2}$, as shown in Equation (2), with the conditions at 25 ºC defined by Equation (3):

$$Ti^{+2} + H_2O \rightleftarrows TiO + 2\,H^+ \qquad (2)$$

$$pH = \frac{10.862 - \log (Ti^{+2}) - \log (H_2O)}{2} \qquad (3)$$

For an aqueous $Ti^{+2}$ activity of $10^{-6}$, the pH values of the precipitation of TiO from $Ti^{+2}$ are 8.51, 8.66, 8.77, and 8.90 for $Br^-$ activities of 15.61, 194.77, 650.06, and 2.042.65, and for water activities of 0.715, 0.358, 0.216, and 0.118, respectively, as shown in Fig. 2a-5a. For each $Br^-$ ion activity, an increase in $Ti^{+2}$ activity from $10^{-6}$ to $10^0$ results in a decrease of the pH value for the formation of TiO from $Ti^{+2}$. In the absence of $Br^-$ ions, TiO is precipitated from $Ti^{+2}$ at a pH value of 8.43, considering a $Ti^{+2}$ activity of $10^{-6}$ and a water activity of 1, as shown in Fig. 1a.

The electrochemical equilibrium between $Ti^{+2}$ and $Ti_2O_3$ is shown in Equation (4). The corresponding Nernst equation at 25 ºC is given by Equation (5):

$$Ti_2O_3 + 6\,H^+ + 2\,e^- \rightleftarrows 2\,Ti^{+2} + 3\,H_2O \quad (4)$$

$$E_{Ti_2O_3/Ti^{+2}}\,(V_{SHE}) = -\,0.480 + 0.0296\,\log\left[\frac{1}{(Ti^{+2})^2\,(H_2O)^3}\right] - 0.177\,pH \quad (5)$$

For each value of the $Ti^{+2}$ activity, the oxidation of $Ti^{+2}$ to form $Ti_2O_3$ occurs at both higher potentials and higher pH values when the bromide ion activity increases and the water activity decreases, as shown in Fig. 2a-5a.

Finally, the precipitation of $TiO_2$ is governed by the electrochemical equilibrium with $Ti^{+2}$ or $Ti^{+3}$, as shown in Equations (6) and (8), respectively. The corresponding Nernst equations at 25 ºC are given by Equations (7) and (9):

$$TiO_2 + 4\,H^+ + 2\,e^- \rightleftarrows Ti^{+2} + 2\,H_2O \quad (6)$$

$$E_{TiO_2/Ti^{+2}}\,(V_{SHE}) = -\,0.518 + 0.0296\,\log\left[\frac{1}{(Ti^{+2})\,(H_2O)^2}\right] - 0.118\,pH \quad (7)$$

$$TiO_2 + 4\,H^+ + e^- \rightleftarrows Ti^{+3} + 2\,H_2O \quad (8)$$

$$E_{TiO_2/Ti^{+3}}\ (V_{SHE}) = -\ 0.664 + 0.0591\ \log\left[\frac{1}{(Ti^{+3})\ (H_2O)^2}\right] - 0.237\ pH \qquad (9)$$

For each activity of the dissolved titanium species, the formation of $TiO_2$ from $Ti^{+2}$ or $Ti^{+3}$ occurs at both higher potentials and higher pH values when the bromide ion activity increases and the water activity decreases, as shown in Fig. 2a-5a.

Neither of the solid titanium bromide species ($TiBr_2$, $TiBr_3$, or $TiBr_4$) are stable at $Br^-$ activities of 15.61, 194.77, 650.06, and 2,042.65.

Predominance diagrams for the dissolved species in Fig. 1a-5a show that the dissolved titanium species at 25 ºC both in the presence and absence of $Br^-$ ions contain oxidation numbers II, III, IV, and VI. The titanium species with valency two is $Ti^{+2}$. The three valent titanium species is $Ti^{+3}$. Oxidation number IV is represented by $TiO^{+2}$ and $HTiO_3^-$. The six valent titanium species is $TiO_2^{+2}$.

Comparison of the simplified Pourbaix diagrams for titanium in $H_2O$ at 25 ºC in the absence and presence of $Br^-$ ions (Fig. 6a-6e) shows that the increase in $Br^-$ activity and the decrease in water activity shift slightly the corrosion area at acid, neutral, and weak alkaline pH to both higher pH values and potentials. The passivation area decreases slightly and the immunity area increases slightly with increasing $Br^-$ activity and decreasing water activity. The size of the pH-independent corrosion area at high potentials remains constant with increasing $Br^-$ activity and decreasing water activity.

*4.2. Pourbaix diagrams for titanium in concentrated aqueous LiBr solutions considering the titanium hydrides*

The generation of hydrogen is one of the relevant problems in the absorption plants, which can have an influence on the formation of metallic hydrides in these systems. Therefore, it can be important to know the conditions of immunity, passivation, and corrosion for titanium in concentrated aqueous LiBr solutions in the presence of titanium hydrides.

Comparison of the Pourbaix diagrams of the simple Ti-$H_2O$ system at 25 ºC not considering and considering the titanium hydrides (Fig. 1a and 1b, respectively) shows that the titanium immunity area and the TiO passivation area disappear in the presence of titanium hydrides. Solid $TiH_2$ is the stable species at low potentials, forming a wide passivation area and reducing the size of the corrosion area at acid pH. $TiH_2$ corrodes in acid solutions to form $Ti^{+2}$. An increase in the activity of $Ti^{+2}$ from $10^{-6}$ to $10^{0}$ results in an increase of electrochemical potential for a given pH value at which there is equilibrium between $TiH_2$ and $Ti^{+2}$. In neutral and alkaline solutions $TiH_2$ oxidizes to form solid $Ti_2O_3$.

Pourbaix diagrams of Ti-$Br^-$-$H_2O$ system at 25 ºC considering the titanium hydrides (Fig. 2b-5b) show that the titanium solubility range in the acid area of the diagrams extends slightly to both higher pH values and potentials with increasing bromide ion activity and decreasing water activity, as a result of destabilization of the solid species $Ti_2O_3$, and $TiO_2$.

Comparison of the simplified Pourbaix diagrams for titanium in $H_2O$ at 25 ºC considering the titanium hydrides in the absence and presence of $Br^-$ ions (Fig. 7a-7e) shows that the increase in $Br^-$ activity and the decrease in water activity shift slightly the corrosion area at acid pH to both higher pH values and potentials. The passivation area decreases slightly with increasing $Br^-$ activity and decreasing water activity. The size of the pH-independent corrosion area at high potentials remains constant with increasing $Br^-$ activity and decreasing water activity.

Pourbaix diagrams for titanium in concentrated aqueous LiBr solutions of 400 g/L, 700 g/L, 850 g/L, and 992 g/L at 25 ºC in the absence and presence of titanium hydrides with precise delineation of the immunity, passivation, and corrosion regions provide significant data to better understand the corrosion behaviour of titanium in refrigeration systems [8,13,15,26,30].

## 5. Conclusions

1. This work has described the construction of Pourbaix diagrams for titanium in concentrated aqueous LiBr solutions of 400 g/L, 700 g/L, 850 g/L, and 992 g/L at 25 ºC in the absence and presence of titanium hydrides, using $Br^-$ activities of 15.61, 194.77, 650.06, and 2,042.65, and water activities of 0.715, 0.358, 0.216, and 0.118, respectively, and dissolved titanium species activities of $10^{-6}$, $10^{-4}$, $10^{-2}$, and $10^{0}$, which have not been reported in the literature. Pourbaix diagrams for titanium in concentrated aqueous LiBr solutions could be particularly useful to study the corrosion behaviour of titanium in refrigeration systems.

2. Comparison of the Pourbaix diagrams of the Ti-$Br^-$-$H_2O$ system at 25 ºC in 400 g/L, 700 g/L, 850 g/l, and 992 g/L LiBr with the diagram of simple Ti-$H_2O$ system at 25 ºC shows that:

    A. The titanium solubility range in the acid, neutral, and weak alkaline areas of the diagrams extends slightly to both higher pH values and potentials with increasing bromide ion activity and decreasing water activity, as a result of destabilization of the solid species TiO, $Ti_2O_3$, and $TiO_2$.

    B. The passivation area decreases slightly and the immunity area increases slightly with increasing $Br^-$ activity and decreasing water activity. The size of the pH-independent corrosion area at high potentials remains constant with increasing $Br^-$ activity and decreasing water activity.

    C. The titanium immunity area and the TiO passivation area disappear in the presence of titanium hydrides. Solid $TiH_2$ is the stable species at low potentials, forming a wide passivation area and reducing the size of the corrosion area at acid pH.

**Acknowledgements**

The authors acknowledge the MICINN (Ministerio de Ciencia e Innovación, Convention no. CTQ2009-07518) and FEDER (Fondo Europeo de Desarrollo Regional) for the support of this work, Dra. M. Asunción Jaime for her translation assistance, and Antonio Juncos for his assistance in plotting the diagrams.

**References**


[1]. J.W. Furlong, Ozone-friendly chiller boasts many advantages, The Air Pollution Consultant 11/12 (1994) 1.12-1.14.

[2]. A.D. Althouse, C.H. Turnquist, A.F. Bracciano, Modern Refrigeration and Air Conditioning, eighteenth ed., Goodheart-Willcox, Illinois, 2004.

[3]. S-F. Lee, S.A. Sherif, Second-law analysis of multi-effect lithium bromide/water absorption chillers, ASHRAE Trans. 105 (1999) 1256-1266.

[4]. F.A. Holland, Clean water through appropriate technology transfer, Appl. Therm. Eng. 20 (2000) 863-871.

[5]. J. Siqueiros, R.J. Romero, Increase of COP for heat transformer in water purification systems. Part I - Increasing heat source temperature, Appl. Therm. Eng. 27 (2007) 1043-1053.

[6]. R.J. Romero, J. Siqueiros, A. Huicochea, Increase of COP for heat transformer in water purification systems. Part II - Without increasing heat source temperature, Appl. Therm. Eng. 27 (2007) 1054-1061.

[7]. J. García-Antón, V. Pérez-Herranz, J.L. Guiñón, G. Lacoste, Use of differential pulse polarography to study corrosion of galvanized steel in aqueous lithium bromide solution, Corrosion 50 (1994) 91-97.

[8]. J.L. Guiñón, J. García-Antón, V. Pérez-Herranz, G. Lacoste, Corrosion of carbon-steels, stainless-steels, and titanium in aqueous lithium bromide solution, Corrosion 50 (1994) 240-246.

[9]. D. Itzhak, T. Greenberg, Galvanic corrosion of a copper alloy in lithium bromide heavy brine environments, Corrosion 55 (1999) 795-799.

[10]. A. Igual-Muñoz, J. García-Antón, J.L. Guiñón, V. Pérez-Herranz, Galvanic study of zinc and copper in lithium bromide solutions at different temperatures, Corrosion 57 (2001) 516-522.

[11]. V. Pérez-Herranz, M.T. Montañés, J. García-Antón, J.L. Guiñón, Effect of fluid velocity and exposure time on copper corrosion in a concentrated lithium bromide solution, Corrosion 57 (2001) 835-842.

[12]. A. Igual-Muñoz, J. García-Antón, J.L. Guiñón, V. Pérez-Herranz, Corrosion behavior and galvanic studies of brass and bronzes in aqueous lithium bromide solutions, Corrosion 58 (2002) 560-569.

[13]. A. Igual-Muñoz, J. García-Antón, J.L. Guiñón, V. Pérez-Herranz, Galvanic studies of copper coupled to alloy 33 and titanium in lithium bromide solutions, Corrosion 58 (2002) 995-1003.

[14]. A. Igual-Muñoz, J. García-Antón, J.L. Guiñón, V. Pérez-Herranz, Effect of aqueous lithium bromide solutions on the corrosion resistance and galvanic behavior of copper-nickel alloys, Corrosion 59 (2003) 32-41.

[15]. A. Igual-Muñoz, J. García-Antón, J.L. Guiñón, V. Pérez-Herranz, Corrosion behavior and galvanic coupling of stainless steels, titanium, and Alloy 33 in lithium bromide solutions, Corrosion 59 (2003) 606-615.

[16]. A. Igual-Muñoz, J. García-Antón, J.L. Guiñón, V. Pérez-Herranz, Corrosion behavior of austenitic and duplex stainless steel weldings in aqueous lithium bromide solution, Corrosion 60 (2004) 982-995.

[17]. A. Igual-Muñoz, J. García-Antón, J.L. Guiñón, V. Pérez-Herranz, Corrosion studies of austenitic and duplex stainless steels in aqueous lithium bromide solution at different temperatures, Corros. Sci. 46 (2004) 2955-2974.

[18]. M.J. Muñoz-Portero, J. García-Antón, J.L. Guiñón, V. Pérez-Herranz, Anodic polarization behavior of copper in concentrated aqueous lithium bromide solutions and comparison with Pourbaix diagrams, Corrosion 61 (2005) 464-472.

[19]. M.T. Montañés, V. Pérez-Herranz, J. García-Antón, J.L. Guiñón, Evolution with exposure time of copper corrosion in a concentrated lithium bromide solution. Characterization of corrosion products by energy-dispersive X-ray analysis and X-ray diffraction, Corrosion 62 (2006) 64-73.

[20]. E. Blasco-Tamarit, A. Igual-Muñoz, J. García-Antón, D. García-García, Effect of aqueous LiBr solutions on the corrosion resistance and galvanic corrosion of an austenitic stainless steel in its welded and non-welded condition, Corros. Sci. 48 (2006) 863-886.

[21]. D.M. García-García, J. García-Antón, A. Igual-Munoz, E. Blasco-Tamarit, Effect of cavitation on the corrosion behaviour of welded and non-welded duplex stainless steel in aqueous LiBr solutions, Corros. Sci. 48 (2006) 2380-2405.

[22]. A. Igual-Muñoz, J. García-Antón, J.L. Guiñón, V. Pérez-Herranz, Effects of solution temperature on localized corrosion of high nickel content stainless steels and nickel in chromated LiBr solution, Corros. Sci. 48 (2006) 3349-3374.

[23]. A. Valero-Gómez, J. García-Antón, A. Igual-Muñoz, Corrosion behavior of copper-phosphorus-silver brazing alloys in lithium bromide solutions, Corrosion 62 (2006) 751-764.

[24]. M.J. Muñoz-Portero, J. García-Antón, J.L. Guiñón, V. Pérez-Herranz, Corrosion of copper in aqueous lithium bromide concentrated solutions by immersion testing, Corrosion 62 (2006) 1018-1027.

[25]. A. Valero-Gomez, A. Igual-Munoz, J. García-Antón, Corrosion and galvanic behavior of copper and copper-brazed joints in heavy brine lithium bromide solutions, Corrosion 62 (2006) 1117-1131.

[26]. E. Blasco-Tamarit, A. Igual-Muñoz, J. García-Antón, D. García-García, Corrosion behaviour and galvanic coupling of titanium and welded titanium in LiBr solutions, Corros. Sci. 49 (2007) 1000-1026.

[27]. D.M. García-García, J. García-Antón, A. Igual-Muñoz, E. Blasco-Tamarit, Cavitation-corrosion studies on welded and nonwelded duplex stainless steel in aqueous lithium bromide solutions, Corrosion 63 (2007) 462-479.

[28]. E. Blasco-Tamarit, A. Igual-Muñoz, J. García-Antón, Galvanic corrosion of high alloyed austenitic stainless steel welds in LiBr systems, Corros. Sci. 49 (2007) 4452-4471.

[29]. D.M. García-García, J. García-Anton, A. Igual-Muñoz, Influence of cavitation on the passive behaviour of duplex stainless steels in aqueous LiBr solutions, Corros. Sci. 50 (2008) 2560-2571.

[30]. E. Blasco-Tamarit, A. Igual-Muñoz, J. García-Antón, D. García-García, Galvanic corrosion of titanium coupled to welded titanium in LiBr solutions at different temperatures, Corros. Sci. 51 (2009) 1095-1102.

[31]. V. Guiñón-Pina, A. Igual-Muñoz, J. García-Antón, Influence of temperature and applied potential on the electrochemical behaviour of nickel in LiBr solutions by

means of electrochemical impedance spectroscopy, Corros. Sci. 51 (2009) 2406-2415.

[32]. M.T. Montañés, R. Sánchez-Tovar, J. García-Antón, V. Pérez-Herranz, The influence of Reynolds number on the galvanic corrosion of the copper/AISI 304 pair in aqueous LiBr solutions, Corros. Sci. 51 (2009) 2733-2742.

[33]. R. Sánchez-Tovar, M.T. Montañés, J. García-Antón, The effect of temperature on the galvanic corrosion of the copper/AISI 304 pair in LiBr solutions under hydrodynamic conditions, Corros. Sci. 52 (2010) 722-733.

[34]. R. Leiva-García, M.J. Muñoz-Portero, J. García-Antón, Corrosion behaviour of sensitized and unsensitized Alloy 900 (UNS 1.4462) in concentrated aqueous lithium bromide solutions at different temperatures, Corros. Sci. 52 (2010) 950-959.

[35]. R. Sanchez-Tovar, M.T. Montañés, J. García-Antón, Effect of different micro-plasma arc welding (MPAW) processes on the corrosion of AISI 316L SS tubes in LiBr and $H_3PO_4$ solutions under flowing conditions, Corros. Sci. 52 (2010) 1508-1519.

[36]. R. M. Fernández-Domene, E. Blasco-Tamarit, D.M. García-García, J. García-Antón, Repassivation of the damage generated by cavitation on UNS N08031 in a LiBr solution by means of electrochemical techniques and Confocal Laser Scanning Microscopy, Corros. Sci. 52 (2010) 3453-3464.

[37]. H.M. Sabir, I.W. Eames, K.O. Suen, The effect of non-condensable gases on the performance of film absorbers in vapour absorption systems, Appl. Therm. Eng. 19 (1999) 531-541.

[38]. H.M Sabir, I.W. Eames, Performance of film absorbers under the effect of a contaminant non-absorbable gas, Appl. Energ. 63 (1999) 255-267.

[39]. Q. Yang, J.L. Luo, The hydrogen-enhanced effects of chloride ions on the passivity of type 304 stainless steel, Electrochim. Acta 45 (2000) 3927-3937.

[40]. J.G. Yu, J.L. Luo, P.R. Norton, Effects of hydrogen on the electronic properties and stability of the passive films on iron, Appl. Surf. Sci. 177 (2001) 129-138.

[41]. M. Pourbaix, Atlas of Electrochemical Equilibria in Aqueous Solutions, first ed., Pergamon Press, New York, 1966.

[42]. ASM Handbook, vol. 13: Corrosion, ninth ed., ASM International, Materials Park, Ohio, 1996.

[43]. M.G. Fontana, Corrosion Engineering, third ed., McGraw-Hill, New York, 1988.

[44]. E. Otero Huerta, Corrosion and Degradation of Materials, Síntesis, Madrid, 1997.

[45]. S. Kesavan, T.A. Mozhi, B.E. Wilde, Potential-pH diagrams for the Fe-$Cl^-$-$H_2O$ system at 25 to 150 C, Corrosion 45 (1989) 213-215.

[46]. A. Anderko, S.J. Sanders, R.D. Young, Real-solution stability diagrams: a thermodynamic tool for modeling corrosion in wide temperature and concentration ranges, Corrosion 53 (1997) 43-53.

[47]. O.V. Kurov, Plotting alloy corrosion state diagrams, Corrosion 57 (2001) 502-507.

[48]. M.J. Muñoz-Portero, J. García-Antón, J.L. Guiñón, V. Pérez-Herranz, Pourbaix diagrams for copper in aqueous lithium bromide concentrated solutions, Corrosion 60 (2004) 749-756.

[49]. M.J. Muñoz-Portero, J. García-Antón, J.L. Guiñón, V. Pérez-Herranz, Pourbaix diagrams for nickel in concentrated aqueous lithium bromide solutions at 25 ºC, Corrosion 63 (2007) 625-634.

[50]. M.J. Muñoz-Portero, J. García-Antón, J.L. Guiñón, V. Pérez-Herranz, Pourbaix diagrams for chromium in concentrated aqueous lithium bromide solutions at 25 ºC, Corros. Sci. 51 (2009) 807-819.

[51]. A.J. Bard, R. Parsons, J. Jordan, Standard Potentials in aqueous solution, Marcel Dekker, New York, 1985.

[52]. C.L. Kusik, H.P. Meissner, Electrolyte activity coefficients in inorganic processing, AIChE Symp. Ser. 74 (1978) 14-20.

[53]. H.P. Meissner, Prediction of activity coefficients of strong electrolytes in aqueous systems, ACS Symp. Ser. 133 (1980) 495-511.

[54]. M.R. Patterson, H. Pérez-Blanco, Numerical fits of the properties of lithium-bromide water solutions, ASHRAE Trans. 94 (1988) 2059-2077.

[55]. C.L. Kusik, H.P. Meissner, Vapor pressures of water over aqueous solutions of strong electrolytes, Ind. Eng. Chem., Process Des. Dev. 12 (1973) 112-115.

**Figures captions**

**Fig. 1.** Pourbaix diagram for the Ti-$H_2O$ system at 25 ºC (a) not considering the titanium hydrides and (b) considering the titanium hydrides.

**Fig. 2.** Pourbaix diagram for the Ti-$Br^-$-$H_2O$ system at 25 ºC for a $Br^-$ activity of 15.61, and a water activity of 0.715 (equivalent to 400 g/L LiBr solution) (a) not considering the titanium hydrides and (b) considering the titanium hydrides.

**Fig. 3.** Pourbaix diagram for the Ti-$Br^-$-$H_2O$ system at 25 ºC for a $Br^-$ activity of 194.77, and a water activity of 0.358 (equivalent to 700 g/L LiBr solution) (a) not considering the titanium hydrides and (b) considering the titanium hydrides.

**Fig. 4.** Pourbaix diagram for the Ti-$Br^-$-$H_2O$ system at 25 ºC for a $Br^-$ activity of 650.06, and a water activity of 0.216 (equivalent to 850 g/L LiBr solution) (a) not considering the titanium hydrides and (b) considering the titanium hydrides.

**Fig. 5.** Pourbaix diagram for the Ti-$Br^-$-$H_2O$ system at 25 ºC for a $Br^-$ activity of 2,042.65, and a water activity of 0.118 (equivalent to 992 g/L LiBr solution) (a) not considering the titanium hydrides and (b) considering the titanium hydrides.

**Fig. 6.** Simplified Pourbaix diagrams for titanium in $H_2O$ at 25 ºC not considering the titanium hydrides (a) in the absence of $Br^-$ ions, (b) for a $Br^-$ activity of 15.61, (c) for a $Br^-$ activity of 194.77, and (d) for a $Br^-$ activity of 650.06, and (e) for a $Br^-$ activity of 2,042.65, considering a $10^{-6}$ activity of the soluble titanium species.

**Fig. 7.** Simplified Pourbaix diagrams for titanium in $H_2O$ at 25 ºC considering the titanium hydrides (a) in the absence of $Br^-$ ions, (b) for a $Br^-$ activity of 15.61, (c) for a $Br^-$ activity of 194.77, and (d) for a $Br^-$ activity of 650.06, and (e) for a $Br^-$ activity of 2,042.65, considering a $10^{-6}$ activity of the soluble titanium species.

**Tables captions**

**Table 1**

Standard Gibbs Free Energies of Formation ($\Delta G_f^o$) at 25 ºC for all the species in the Ti-$Br^-$-$H_2O$ system (aq = aqueous, g = gas, l = liquid, and s = solid) [51]

**Table 2**

Electrochemical reactions involving $H^+$ for the Ti-$Br^-$-$H_2O$ system[(A)]

**Table 2**

Electrochemical reactions involving $H^+$ for the Ti-$Br^-$-$H_2O$ system[(A)] (continuation 1)

**Table 2**

Electrochemical reactions involving $H^+$ for the Ti-$Br^-$-$H_2O$ system[(A)] (continuation 2)

**Table 3**

Electrochemical reactions not involving $H^+$ for the Ti-$Br^-$-$H_2O$ system[(A)]

**Table 4**

Chemical reactions involving $H^+$ for the Ti-$Br^-$-$H_2O$ system[(A)]

**Table 5**

Chemical reactions not involving $H^+$ for the Ti-$Br^-$-$H_2O$ system[(A)]

**Table 6**

Additional electrochemical reactions involving $H^+$ for the Ti-$Br^-$-$H_2O$ system, considering the titanium hydrides[(A)]

**Table 6**

Additional electrochemical reactions involving $H^+$ for the Ti-$Br^-$-$H_2O$ system, considering the titanium hydrides[(A)] (continuation 1)

**Table 7**

Calculated thermodynamic stability of titanium species in the Ti-$Br^-$-$H_2O$ system (a = it appears in the Pourbaix diagram not considering the titanium hydrides; b = it appears in the Pourbaix diagram considering the titanium hydrides)

**Table 1 (revised)**

| Species | Oxidation number[(A)] | State | $\Delta G_f^o$ (kJ/mol) |
|---|---|---|---|
| $H^+$ | | aq | 0 |
| $H_2$ | | g | 0 |
| $O_2$ | | g | 0 |
| $H_2O$ | | l | – 237.178 |
| $OH^-$ | | aq | – 157.293 |
| Ti | 0 | s | 0 |
| $TiH_2$ | II | s | – 4.92 |
| TiH | I | s | – 3.59 |
| TiO | II | s | – 489.2 |
| $Ti_2O_3$ | III | s | – 1432.2 |
| $Ti(OH)_3$ | III | s | – 1049.8 |
| $Ti_3O_5$ | III/IV | s | – 2314 |
| $TiO_2$ | IV | s | – 888.4 |
| $TiO_2 \cdot H_2O$ | IV | s | – 1058.5 |
| $Ti^{+2}$ | II | aq | – 314 |
| $Ti^{+3}$ | III | aq | – 350 |
| $TiO^{+2}$ | IV | aq | – 577.4 |
| $HTiO_3^-$ | IV | aq | – 955.9 |
| $TiO_2^{+2}$ | VI | aq | – 467.2 |
| $Br^-$ | | aq | – 103.97 |
| $TiBr_2$ | II | s | – 382.4 |
| $TiBr_3$ | III | s | – 521.3 |
| $TiBr_4$ | IV | s | – 610.9 |

[(A)] Oxidation number for the titanium species.

**Table 2**

| Type | Equation | Number |
|---|---|---|
| Homogeneous | $TiO^{+2} + 2\,H^{+} + 2\,e^{-} \rightleftarrows Ti^{+2} + H_2O$ | 1 |
| | $HTiO_3^{-} + 5\,H^{+} + 2\,e^{-} \rightleftarrows Ti^{+2} + 3\,H_2O$ | 2 |
| | $TiO_2^{+2} + 4\,H^{+} + 4\,e^{-} \rightleftarrows Ti^{+2} + 2\,H_2O$ | 3 |
| | $TiO^{+2} + 2\,H^{+} + e^{-} \rightleftarrows Ti^{+3} + H_2O$ | 4 |
| | $HTiO_3^{-} + 5\,H^{+} + e^{-} \rightleftarrows Ti^{+3} + 3\,H_2O$ | 5 |
| | $TiO_2^{+2} + 4\,H^{+} + 3\,e^{-} \rightleftarrows Ti^{+3} + 2\,H_2O$ | 6 |
| | $TiO_2^{+2} + 2\,H^{+} + 2\,e^{-} \rightleftarrows TiO^{+2} + H_2O$ | 7 |
| | $TiO_2^{+2} + H_2O + 2\,e^{-} \rightleftarrows HTiO_3^{-} + H^{+}$ | 8 |
| Heterogeneous with two solid species | $\mathbf{TiO} + 2\,H^{+} + 2\,e^{-} \rightleftarrows \mathbf{Ti} + H_2O$ | 9 |
| | $\mathbf{Ti_2O_3} + 6\,H^{+} + 6\,e^{-} \rightleftarrows 2\,\mathbf{Ti} + 3\,H_2O$ | 10 |
| | $\mathbf{Ti(OH)_3} + 3\,H^{+} + 3\,e^{-} \rightleftarrows \mathbf{Ti} + 3\,H_2O$ | 11 |
| | $\mathbf{Ti_3O_5} + 10\,H^{+} + 10\,e^{-} \rightleftarrows 3\,\mathbf{Ti} + 5\,H_2O$ | 12 |
| | $\mathbf{TiO_2} + 4\,H^{+} + 4\,e^{-} \rightleftarrows \mathbf{Ti} + 2\,H_2O$ | 13 |
| | $\mathbf{TiO_2{\cdot}H_2O} + 4\,H^{+} + 4\,e^{-} \rightleftarrows \mathbf{Ti} + 3\,H_2O$ | 14 |
| | $\mathbf{Ti_2O_3} + 2\,H^{+} + 2\,e^{-} \rightleftarrows 2\,\mathbf{TiO} + H_2O$ | 15 |
| | $\mathbf{Ti(OH)_3} + H^{+} + e^{-} \rightleftarrows \mathbf{TiO} + 2\,H_2O$ | 16 |
| | $\mathbf{Ti_3O_5} + 4\,H^{+} + 4\,e^{-} \rightleftarrows 3\,\mathbf{TiO} + 2\,H_2O$ | 17 |
| | $\mathbf{TiO_2} + 2\,H^{+} + 2\,e^{-} \rightleftarrows \mathbf{TiO} + H_2O$ | 18 |
| | $\mathbf{TiO_2{\cdot}H_2O} + 2\,H^{+} + 2\,e^{-} \rightleftarrows \mathbf{TiO} + 2\,H_2O$ | 19 |
| | $\mathbf{TiBr_3} + H_2O + e^{-} \rightleftarrows \mathbf{TiO} + 3\,Br^{-} + 2\,H^{+}$ | 20 |
| | $\mathbf{TiBr_4} + H_2O + 2\,e^{-} \rightleftarrows \mathbf{TiO} + 4\,Br^{-} + 2\,H^{+}$ | 21 |
| | $2\,\mathbf{Ti_3O_5} + 2\,H^{+} + 2\,e^{-} \rightleftarrows 3\,\mathbf{Ti_2O_3} + H_2O$ | 22 |
| | $2\,\mathbf{TiO_2} + 2\,H^{+} + 2\,e^{-} \rightleftarrows \mathbf{Ti_2O_3} + H_2O$ | 23 |
| | $2\,\mathbf{TiO_2{\cdot}H_2O} + 2\,H^{+} + 2\,e^{-} \rightleftarrows \mathbf{Ti_2O_3} + 3\,H_2O$ | 24 |
| | $\mathbf{Ti_2O_3} + 4\,Br^{-} + 6\,H^{+} + 2\,e^{-} \rightleftarrows 2\,\mathbf{TiBr_2} + 3\,H_2O$ | 25 |
| | $2\,\mathbf{TiBr_4} + 3\,H_2O + 2\,e^{-} \rightleftarrows \mathbf{Ti_2O_3} + 8\,Br^{-} + 6\,H^{+}$ | 26 |
| | $\mathbf{Ti_3O_5} + H^{+} + 4\,H_2O + e^{-} \rightleftarrows 3\,\mathbf{Ti(OH)_3}$ | 27 |
| | $\mathbf{TiO_2} + H^{+} + H_2O + e^{-} \rightleftarrows \mathbf{Ti(OH)_3}$ | 28 |

**Table 2 (continuation 1)**

| Type | Equation | Number |
|---|---|---|
| Heterogeneous with two solid species | $\mathbf{TiO_2{\cdot}H_2O} + H^+ + e^- \rightleftarrows \mathbf{Ti(OH)_3}$ | 29 |
| | $\mathbf{Ti(OH)_3} + 2\,Br^- + 3\,H^+ + e^- \rightleftarrows \mathbf{TiBr_2} + 3\,H_2O$ | 30 |
| | $\mathbf{TiBr_4} + 3\,H_2O + e^- \rightleftarrows \mathbf{Ti(OH)_3} + 4\,Br^- + 3\,H^+$ | 31 |
| | $3\,\mathbf{TiO_2} + 2\,H^+ + 2\,e^- \rightleftarrows \mathbf{Ti_3O_5} + H_2O$ | 32 |
| | $3\,\mathbf{TiO_2{\cdot}H_2O} + 2\,H^+ + 2\,e^- \rightleftarrows \mathbf{Ti_3O_5} + 4\,H_2O$ | 33 |
| | $\mathbf{Ti_3O_5} + 6\,Br^- + 10\,H^+ + 4\,e^- \rightleftarrows 3\,\mathbf{TiBr_2} + 5\,H_2O$ | 34 |
| | $\mathbf{Ti_3O_5} + 9\,Br^- + 10\,H^+ + e^- \rightleftarrows 3\,\mathbf{TiBr_3} + 5\,H_2O$ | 35 |
| | $3\,\mathbf{TiBr_4} + 5\,H_2O + 2\,e^- \rightleftarrows \mathbf{Ti_3O_5} + 12\,Br^- + 10\,H^+$ | 36 |
| | $\mathbf{TiO_2} + 2\,Br^- + 4\,H^+ + 2\,e^- \rightleftarrows \mathbf{TiBr_2} + 2\,H_2O$ | 37 |
| | $\mathbf{TiO_2} + 3\,Br^- + 4\,H^+ + e^- \rightleftarrows \mathbf{TiBr_3} + 2\,H_2O$ | 38 |
| | $\mathbf{TiO_2{\cdot}H_2O} + 2\,Br^- + 4\,H^+ + 2\,e^- \rightleftarrows \mathbf{TiBr_2} + 3\,H_2O$ | 39 |
| | $\mathbf{TiO_2{\cdot}H_2O} + 3\,Br^- + 4\,H^+ + e^- \rightleftarrows \mathbf{TiBr_3} + 3\,H_2O$ | 40 |
| Heterogeneous with one solid species | $TiO^{+2} + 2\,H^+ + 4\,e^- \rightleftarrows \mathbf{Ti} + H_2O$ | 41 |
| | $HTiO_3^- + 5\,H^+ + 4\,e^- \rightleftarrows \mathbf{Ti} + 3\,H_2O$ | 42 |
| | $TiO_2^{+2} + 4\,H^+ + 6\,e^- \rightleftarrows \mathbf{Ti} + 2\,H_2O$ | 43 |
| | $Ti^{+3} + H_2O + e^- \rightleftarrows \mathbf{TiO} + 2\,H^+$ | 44 |
| | $HTiO_3^- + 3\,H^+ + 2\,e^- \rightleftarrows \mathbf{TiO} + 2\,H_2O$ | 45 |
| | $TiO_2^{+2} + 2\,H^+ + 4\,e^- \rightleftarrows \mathbf{TiO} + H_2O$ | 46 |
| | $\mathbf{Ti_2O_3} + 6\,H^+ + 2\,e^- \rightleftarrows 2\,Ti^{+2} + 3\,H_2O$ | 47 |
| | $2\,TiO^{+2} + H_2O + 2\,e^- \rightleftarrows \mathbf{Ti_2O_3} + 2\,H^+$ | 48 |
| | $2\,HTiO_3^- + 4\,H^+ + 2\,e^- \rightleftarrows \mathbf{Ti_2O_3} + 3\,H_2O$ | 49 |
| | $2\,TiO_2^{+2} + 2\,H^+ + 6\,e^- \rightleftarrows \mathbf{Ti_2O_3} + H_2O$ | 50 |
| | $\mathbf{Ti(OH)_3} + 3\,H^+ + e^- \rightleftarrows Ti^{+2} + 3\,H_2O$ | 51 |
| | $TiO^{+2} + 2\,H_2O + e^- \rightleftarrows \mathbf{Ti(OH)_3} + H^+$ | 52 |
| | $HTiO_3^- + 2\,H^+ + e^- \rightleftarrows \mathbf{Ti(OH)_3}$ | 53 |
| | $TiO_2^{+2} + H^+ + H_2O + 3\,e^- \rightleftarrows \mathbf{Ti(OH)_3}$ | 54 |
| | $\mathbf{Ti_3O_5} + 10\,H^+ + 4\,e^- \rightleftarrows 3\,Ti^{+2} + 5\,H_2O$ | 55 |
| | $\mathbf{Ti_3O_5} + 10\,H^+ + e^- \rightleftarrows 3\,Ti^{+3} + 5\,H_2O$ | 56 |
| | $3\,TiO^{+2} + 2\,H_2O + 2\,e^- \rightleftarrows \mathbf{Ti_3O_5} + 4\,H^+$ | 57 |

**Table 2 (continuation 2)**

| Type | Equation | Number |
|---|---|---|
| Heterogeneous with one solid species | $3\,HTiO_3^- + 5\,H^+ + 2\,e^- \rightleftarrows \mathbf{Ti_3O_5} + 4\,H_2O$ | 58 |
| | $3\,TiO_2^{+2} + 2\,H^+ + 8\,e^- \rightleftarrows \mathbf{Ti_3O_5} + H_2O$ | 59 |
| | $\mathbf{TiO_2} + 4\,H^+ + 2\,e^- \rightleftarrows Ti^{+2} + 2\,H_2O$ | 60 |
| | $\mathbf{TiO_2} + 4\,H^+ + e^- \rightleftarrows Ti^{+3} + 2\,H_2O$ | 61 |
| | $\mathbf{TiO_2{\cdot}H_2O} + 4\,H^+ + 2\,e^- \rightleftarrows Ti^{+2} + 3\,H_2O$ | 62 |
| | $\mathbf{TiO_2{\cdot}H_2O} + 4\,H^+ + e^- \rightleftarrows Ti^{+3} + 3\,H_2O$ | 63 |
| | $TiO^{+2} + 2\,Br^- + 2\,H^+ + 2\,e^- \rightleftarrows \mathbf{TiBr_2} + H_2O$ | 64 |
| | $TiO^{+2} + 3\,Br^- + 2\,H^+ + e^- \rightleftarrows \mathbf{TiBr_3} + H_2O$ | 65 |
| | $HTiO_3^- + 2\,Br^- + 5\,H^+ + 2\,e^- \rightleftarrows \mathbf{TiBr_2} + 3\,H_2O$ | 66 |
| | $HTiO_3^- + 3\,Br^- + 5\,H^+ + e^- \rightleftarrows \mathbf{TiBr_3} + 3\,H_2O$ | 67 |
| | $TiO_2^{+2} + 2\,Br^- + 4\,H^+ + 4\,e^- \rightleftarrows \mathbf{TiBr_2} + 2\,H_2O$ | 68 |
| | $TiO_2^{+2} + 3\,Br^- + 4\,H^+ + 3\,e^- \rightleftarrows \mathbf{TiBr_3} + 2\,H_2O$ | 69 |
| | $TiO_2^{+2} + 4\,Br^- + 4\,H^+ + 2\,e^- \rightleftarrows \mathbf{TiBr_4} + 2\,H_2O$ | 70 |

(A) Solid species are typed in bold letters. Reactions used for the construction of the Pourbaix diagram for the simple Ti-$H_2O$ system are shaded.

**Table 3**

| Type | Equation | Number |
|---|---|---|
| Homogeneous | $Ti^{+3} + e^- \rightleftarrows Ti^{+2}$ | 71 |
| Heterogeneous with two solid species | $\mathbf{TiBr_2} + 2\,e^- \rightleftarrows \mathbf{Ti} + 2\,Br^-$ | 72 |
| | $\mathbf{TiBr_3} + 3\,e^- \rightleftarrows \mathbf{Ti} + 3\,Br^-$ | 73 |
| | $\mathbf{TiBr_4} + 4\,e^- \rightleftarrows \mathbf{Ti} + 4\,Br^-$ | 74 |
| | $\mathbf{TiBr_3} + e^- \rightleftarrows \mathbf{TiBr_2} + Br^-$ | 75 |
| | $\mathbf{TiBr_4} + 2\,e^- \rightleftarrows \mathbf{TiBr_2} + 2\,Br^-$ | 76 |
| | $\mathbf{TiBr_4} + e^- \rightleftarrows \mathbf{TiBr_3} + Br^-$ | 77 |
| Heterogeneous with one solid species | $Ti^{+2} + 2\,e^- \rightleftarrows \mathbf{Ti}$ | 78 |
| | $Ti^{+3} + 3\,e^- \rightleftarrows \mathbf{Ti}$ | 79 |
| | $TiO^{+2} + 2\,e^- \rightleftarrows \mathbf{TiO}$ | 80 |
| | $TiO_2^{+2} + 2\,e^- \rightleftarrows \mathbf{TiO_2}$ | 81 |
| | $TiO_2^{+2} + H_2O + 2\,e^- \rightleftarrows \mathbf{TiO_2{\cdot}H_2O}$ | 82 |
| | $\mathbf{TiBr_3} + e^- \rightleftarrows Ti^{+2} + 3\,Br^-$ | 83 |
| | $\mathbf{TiBr_4} + 2\,e^- \rightleftarrows Ti^{+2} + 4\,Br^-$ | 84 |
| | $Ti^{+3} + 2\,Br^- + e^- \rightleftarrows \mathbf{TiBr_2}$ | 85 |
| | $\mathbf{TiBr_4} + e^- \rightleftarrows Ti^{+3} + 4\,Br^-$ | 86 |

(A) Solid species are typed in bold letters. Reactions used for the construction of the Pourbaix diagram for the simple Ti-$H_2O$ system are shaded.

**Table 4**

| Type | Equation | Number |
|---|---|---|
| Homogeneous | $TiO^{+2} + 2\,H_2O \rightleftarrows HTiO_3^- + 3\,H^+$ | 87 |
| Heterogeneous with two solid species | $\mathbf{TiBr_2} + H_2O \rightleftarrows \mathbf{TiO} + 2\,Br^- + 2\,H^+$ | 88 |
| | $2\,\mathbf{TiBr_3} + 3\,H_2O \rightleftarrows \mathbf{Ti_2O_3} + 6\,Br^- + 6\,H^+$ | 89 |
| | $\mathbf{TiBr_3} + 3\,H_2O \rightleftarrows \mathbf{Ti(OH)_3} + 3\,Br^- + 3\,H^+$ | 90 |
| | $\mathbf{TiBr_4} + 2\,H_2O \rightleftarrows \mathbf{TiO_2} + 4\,Br^- + 4\,H^+$ | 91 |
| | $\mathbf{TiBr_4} + 3\,H_2O \rightleftarrows \mathbf{TiO_2{\cdot}H_2O} + 4\,Br^- + 4\,H^+$ | 92 |
| Heterogeneous with one solid species | $Ti^{+2} + H_2O \rightleftarrows \mathbf{TiO} + 2\,H^+$ | 93 |
| | $2\,Ti^{+3} + 3\,H_2O \rightleftarrows \mathbf{Ti_2O_3} + 6\,H^+$ | 94 |
| | $Ti^{+3} + 3\,H_2O \rightleftarrows \mathbf{Ti(OH)_3} + 3\,H^+$ | 95 |
| | $TiO^{+2} + H_2O \rightleftarrows \mathbf{TiO_2} + 2\,H^+$ | 96 |
| | $\mathbf{TiO_2} + H_2O \rightleftarrows HTiO_3^- + H^+$ | 97 |
| | $TiO^{+2} + 2\,H_2O \rightleftarrows \mathbf{TiO_2{\cdot}H_2O} + 2\,H^+$ | 98 |
| | $\mathbf{TiO_2{\cdot}H_2O} \rightleftarrows HTiO_3^- + H^+$ | 99 |
| | $\mathbf{TiBr_4} + H_2O \rightleftarrows TiO^{+2} + 4\,Br^- + 2\,H^+$ | 100 |
| | $\mathbf{TiBr_4} + 3\,H_2O \rightleftarrows HTiO_3^- + 4\,Br^- + 5\,H^+$ | 101 |

(A) Solid species are typed in bold letters. Reactions used for the construction of the Pourbaix diagram for the simple Ti-$H_2O$ system are shaded.

**Table 5**

| Type | Equation | Number |
|---|---|---|
| Heterogeneous with two solid species | $\mathbf{Ti_2O_3} + 3\,H_2O \rightleftarrows 2\,\mathbf{Ti(OH)_3}$ | 102 |
| | $\mathbf{TiO_2} + H_2O \rightleftarrows \mathbf{TiO_2{\cdot}H_2O}$ | 103 |
| Heterogeneous with one solid species | $Ti^{+2} + 2\,Br^- \rightleftarrows \mathbf{TiBr_2}$ | 104 |
| | $Ti^{+3} + 3\,Br^- \rightleftarrows \mathbf{TiBr_3}$ | 105 |

(A) Solid species are typed in bold letters. Reactions used for the construction of the Pourbaix diagram for the simple Ti-$H_2O$ system are shaded.

**Table 6**

| Type | Equation | Number |
|---|---|---|
| Heterogeneous with two solid species | $\mathbf{Ti} + 2\,H^+ + 2\,e^- \rightleftarrows \mathbf{TiH_2}$ | 106 |
| | $\mathbf{Ti} + H^+ + e^- \rightleftarrows \mathbf{TiH}$ | 107 |
| | $\mathbf{TiH} + H^+ + e^- \rightleftarrows \mathbf{TiH_2}$ | 108 |
| | $\mathbf{TiO} + 4\,H^+ + 4\,e^- \rightleftarrows \mathbf{TiH_2} + H_2O$ | 109 |
| | $\mathbf{Ti_2O_3} + 10\,H^+ + 10\,e^- \rightleftarrows 2\,\mathbf{TiH_2} + 3\,H_2O$ | 110 |
| | $\mathbf{Ti(OH)_3} + 5\,H^+ + 5\,e^- \rightleftarrows \mathbf{TiH_2} + 3\,H_2O$ | 111 |
| | $\mathbf{Ti_3O_5} + 16\,H^+ + 16\,e^- \rightleftarrows 3\,\mathbf{TiH_2} + 5\,H_2O$ | 112 |
| | $\mathbf{TiO_2} + 6\,H^+ + 6\,e^- \rightleftarrows \mathbf{TiH_2} + 2\,H_2O$ | 113 |
| | $\mathbf{TiO_2{\cdot}H_2O} + 6\,H^+ + 6\,e^- \rightleftarrows \mathbf{TiH_2} + 3\,H_2O$ | 114 |
| | $\mathbf{TiBr_2} + 2\,H^+ + 4\,e^- \rightleftarrows \mathbf{TiH_2} + 2\,Br^-$ | 115 |
| | $\mathbf{TiBr_3} + 2\,H^+ + 5\,e^- \rightleftarrows \mathbf{TiH_2} + 3\,Br^-$ | 116 |
| | $\mathbf{TiBr_4} + 2\,H^+ + 6\,e^- \rightleftarrows \mathbf{TiH_2} + 4\,Br^-$ | 117 |
| | $\mathbf{TiO} + 3\,H^+ + 3\,e^- \rightleftarrows \mathbf{TiH} + H_2O$ | 118 |
| | $\mathbf{Ti_2O_3} + 8\,H^+ + 8\,e^- \rightleftarrows 2\,\mathbf{TiH} + 3\,H_2O$ | 119 |
| | $\mathbf{Ti(OH)_3} + 4\,H^+ + 4\,e^- \rightleftarrows \mathbf{TiH} + 3\,H_2O$ | 120 |
| | $\mathbf{Ti_3O_5} + 13\,H^+ + 13\,e^- \rightleftarrows 3\,\mathbf{TiH} + 5\,H_2O$ | 121 |
| | $\mathbf{TiO_2} + 5\,H^+ + 5\,e^- \rightleftarrows \mathbf{TiH} + 2\,H_2O$ | 122 |
| | $\mathbf{TiO_2{\cdot}H_2O} + 5\,H^+ + 5\,e^- \rightleftarrows \mathbf{TiH} + 3\,H_2O$ | 123 |
| | $\mathbf{TiBr_2} + H^+ + 3\,e^- \rightleftarrows \mathbf{TiH} + 2\,Br^-$ | 124 |
| | $\mathbf{TiBr_3} + H^+ + 4\,e^- \rightleftarrows \mathbf{TiH} + 3\,Br^-$ | 125 |
| | $\mathbf{TiBr_4} + H^+ + 5\,e^- \rightleftarrows \mathbf{TiH} + 4\,Br^-$ | 126 |
| Heterogeneous with one solid species | $Ti^{+2} + 2\,H^+ + 4\,e^- \rightleftarrows \mathbf{TiH_2}$ | 127 |
| | $Ti^{+3} + 2\,H^+ + 5\,e^- \rightleftarrows \mathbf{TiH_2}$ | 128 |
| | $TiO^{+2} + 4\,H^+ + 6\,e^- \rightleftarrows \mathbf{TiH_2} + H_2O$ | 129 |
| | $HTiO_3^- + 7\,H^+ + 6\,e^- \rightleftarrows \mathbf{TiH_2} + 3\,H_2O$ | 130 |
| | $TiO_2^{+2} + 6\,H^+ + 8\,e^- \rightleftarrows \mathbf{TiH_2} + 2\,H_2O$ | 131 |
| | $Ti^{+2} + H^+ + 3\,e^- \rightleftarrows \mathbf{TiH}$ | 132 |

**Table 6 (continuation 1)**

| Type | Equation | Number |
|---|---|---|
| Heterogeneous with one solid species | $Ti^{+3} + H^{+} + 4\,e^{-} \rightleftarrows \mathbf{TiH}$ | 133 |
| | $TiO^{+2} + 3\,H^{+} + 5\,e^{-} \rightleftarrows \mathbf{TiH} + H_2O$ | 134 |
| | $HTiO_3^{-} + 6\,H^{+} + 5\,e^{-} \rightleftarrows \mathbf{TiH} + 3\,H_2O$ | 135 |
| | $TiO_2^{+2} + 5\,H^{+} + 7\,e^{-} \rightleftarrows \mathbf{TiH} + 2\,H_2O$ | 136 |

(A) Solid species are typed in bold letters. Reactions used for the construction of the Pourbaix diagram for the simple Ti-$H_2O$ system are shaded.

**Table 7**

| Species | $(Br^-) = 0$<br>$(H_2O) = 1$<br>[LiBr] = 0 g/L | $(Br^-) = 15.61$<br>$(H_2O) = 0.715$<br>[LiBr] = 400 g/L | $(Br^-) = 194.77$<br>$(H_2O) = 0.358$<br>[LiBr] = 700 g/L | $(Br^-) = 650.06$<br>$(H_2O) = 0.216$<br>[LiBr] = 850 g/L | $(Br^-) = 2{,}042.65$<br>$(H_2O) = 0.118$<br>[LiBr] = 992 g/L |
|---|---|---|---|---|---|
| Ti | a | a | a | a | a |
| $TiH_2$ | b | b | b | b | b |
| TiH | | | | | |
| TiO | a | a | a | a | a |
| $Ti_2O_3$ | ab | ab | ab | ab | ab |
| $Ti(OH)_3$ | | | | | |
| $Ti_3O_5$ | | | | | |
| $TiO_2$ | ab | ab | ab | ab | ab |
| $TiO_2 \cdot H_2O$ | | | | | |
| $Ti^{+2}$ | ab | ab | ab | ab | ab |
| $Ti^{+3}$ | ab | ab | ab | ab | ab |
| $TiO^{+2}$ | ab | ab | ab | ab | ab |
| $HTiO_3^-$ | ab | ab | ab | ab | ab |
| $TiO_2^{+2}$ | ab | ab | ab | ab | ab |
| $TiBr_2$ | | | | | |
| $TiBr_3$ | | | | | |
| $TiBr_4$ | | | | | |

**Figure 1**

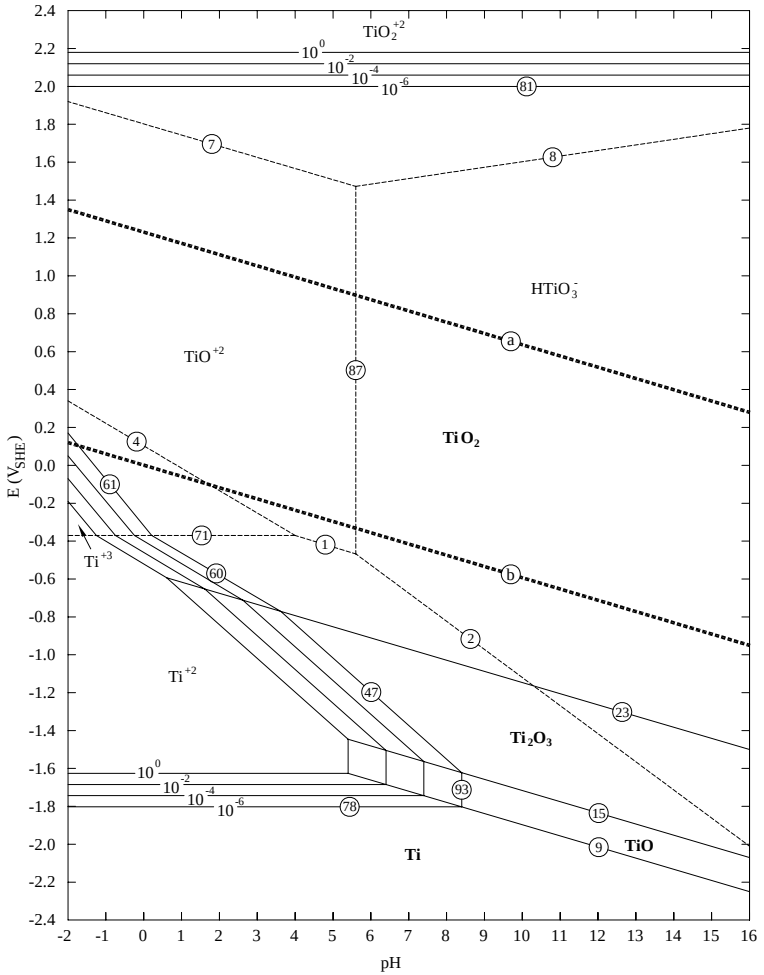
TiO2+2
10 0
10 -2
10 -4
10 -6
81
7
8
HTiO3-
a
TiO +2
87
TiO2
4
61
71
1
Ti +3
b
60
2
Ti +2
47
23
Ti2O3
10 0
10 -2
10 -4
10 -6
93
78
15
9
TiO
Ti
E (VSHE)
pH

(a)

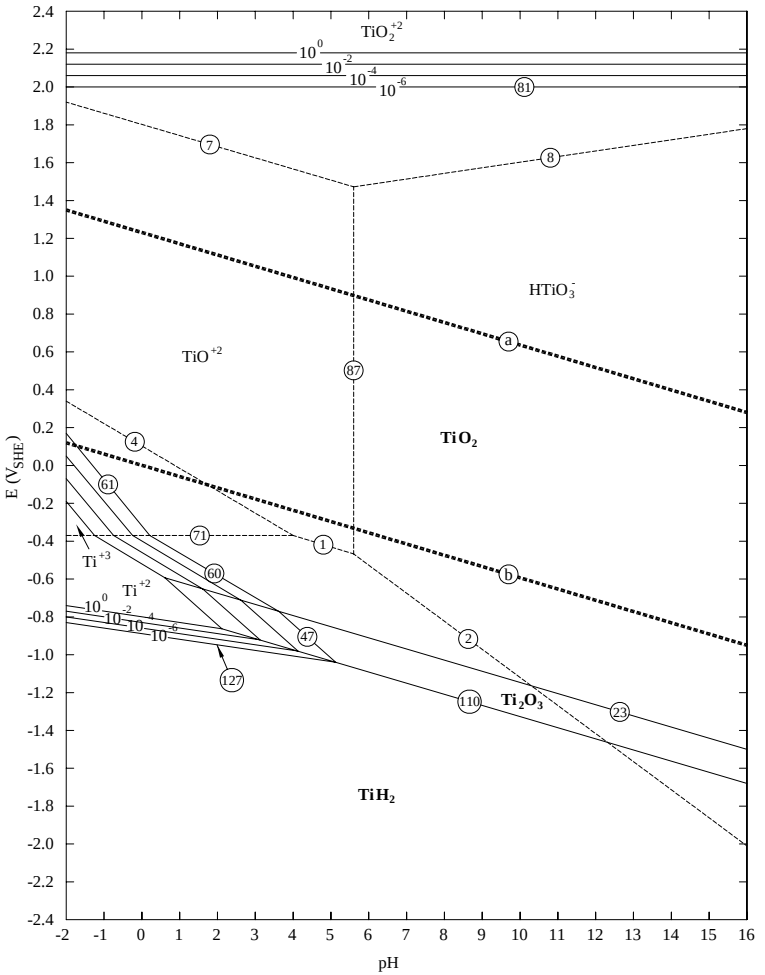
TiO2+2
10 0
10 -2
10 -4
10 -6
81
7
8
HTiO3-
a
TiO +2
87
TiO2
4
61
71
1
Ti +3
b
60
Ti +2
10 0
10 -2
10 -4
10 -6
47
2
127
110
Ti2O3
23
TiH2
E (VSHE)
pH

(b)

**Figure 2**

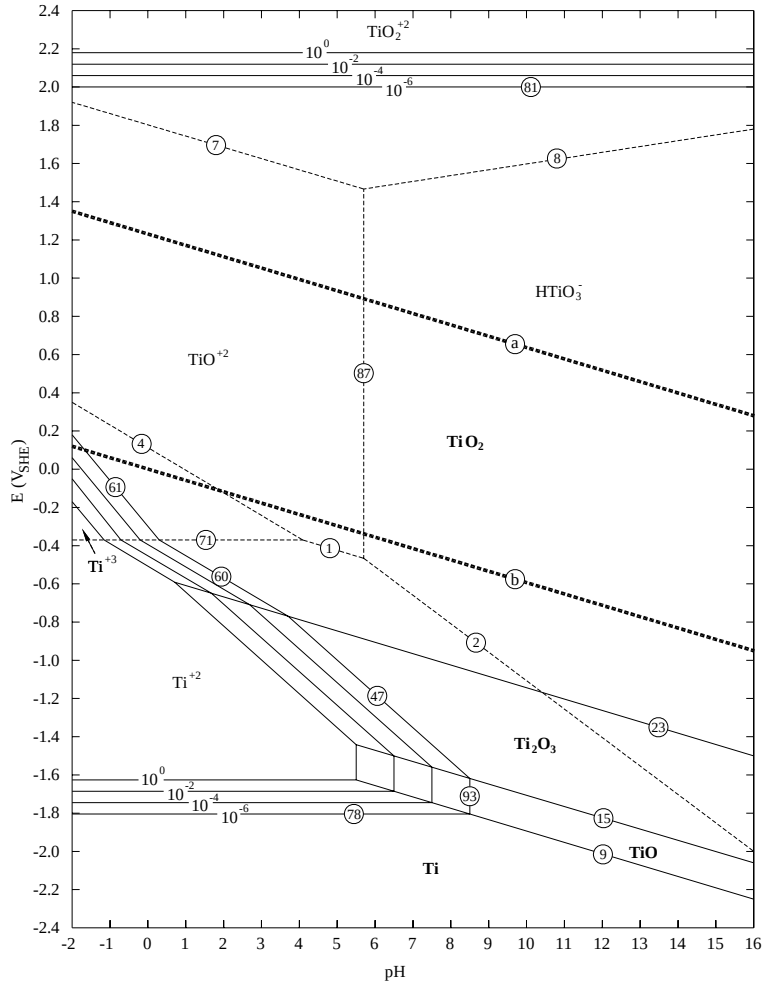
TiO2+2
10 0
10 -2
10 -4
10 -6
81
7
8
HTiO3-
a
TiO+2
87
TiO2
4
61
71
1
Ti+3
b
60
2
Ti+2
47
23
Ti2O3
10 0
10 -2
10 -4
10 -6
93
78
15
9
TiO
Ti
E (VSHE)
pH

(a)

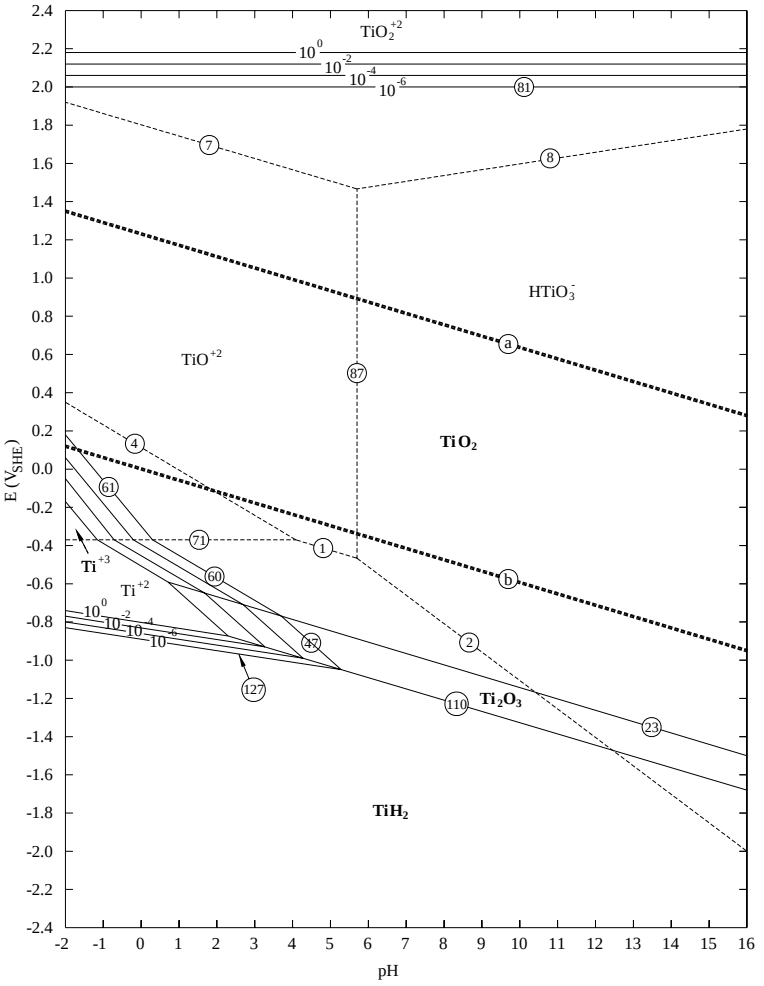
TiO2+2
10 0
10 -2
10 -4
10 -6
81
7
8
HTiO3-
a
TiO+2
87
TiO2
4
61
71
1
Ti+3
b
60
Ti+2
10 0
10 -2
10 -4
10 -6
42
2
127
110
Ti2O3
23
TiH2
E (VSHE)
pH

(b)

**Figure 3**

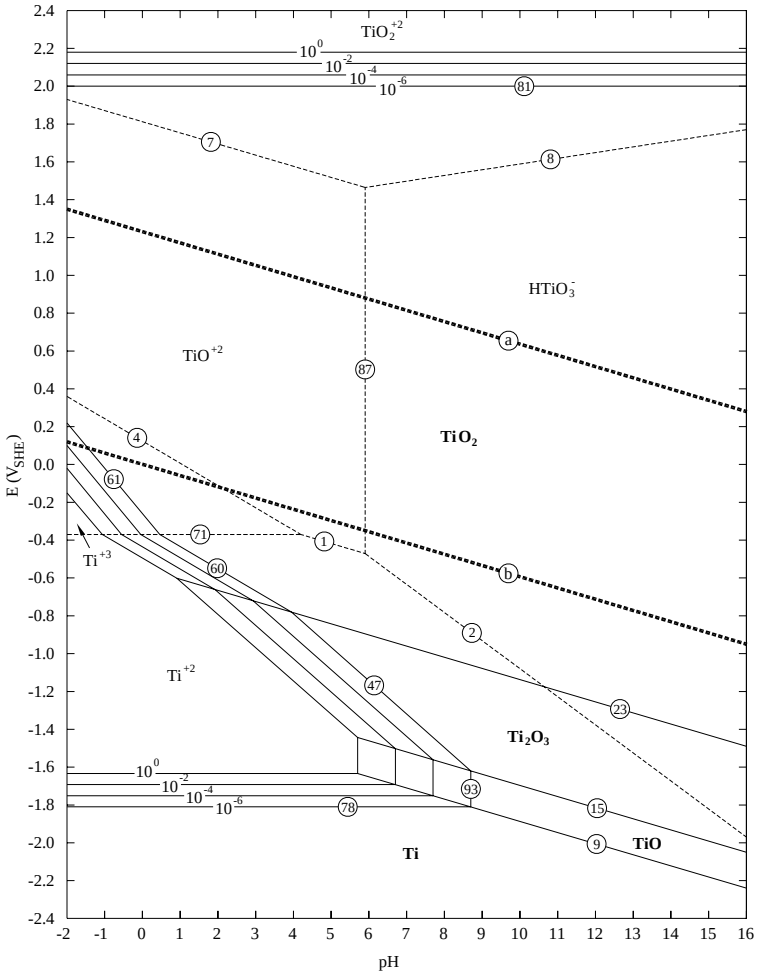
TiO2+2
10 0
10 -2
10 -4
10 -6
81
7
8
HTiO3-
a
TiO+2
87
TiO2
4
61
71
1
Ti+3
60
b
2
Ti+2
47
23
Ti2O3
10 0
10 -2
10 -4
10 -6
93
78
15
9
TiO
Ti
E (VSHE)
pH

(a)

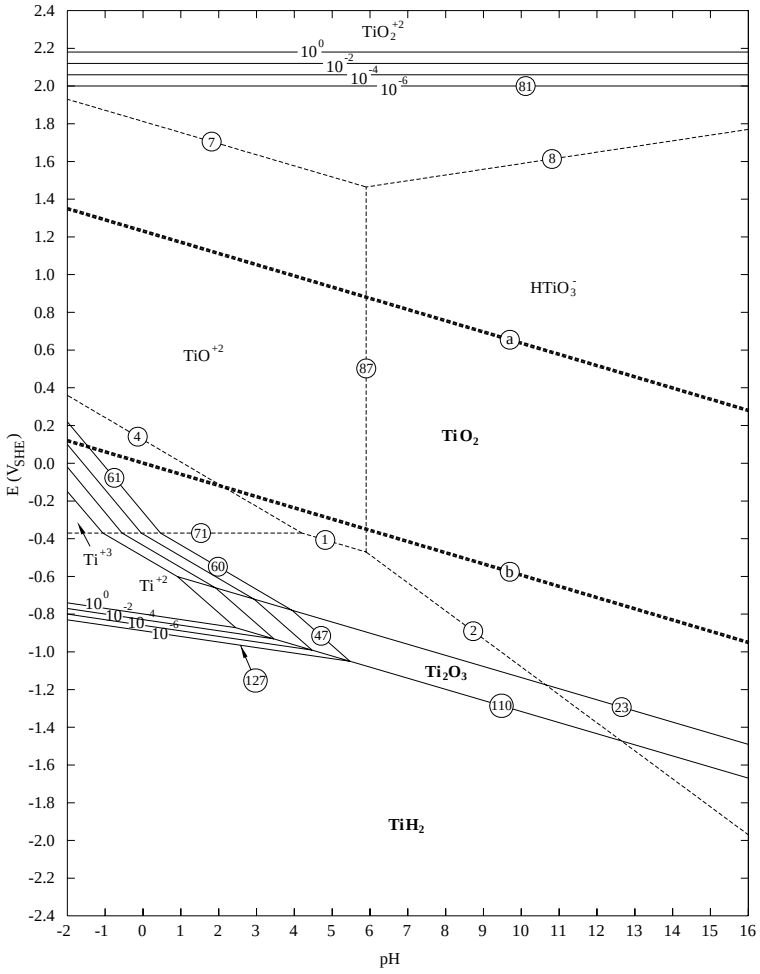
TiO2+2
10 0
10 -2
10 -4
10 -6
81
7
8
HTiO3-
a
TiO+2
87
TiO2
4
61
71
1
Ti+3
60
b
Ti+2
10 0
10 -2
10 -4
10 -6
47
2
127
Ti2O3
110
23
TiH2
E (VSHE)
pH

(b)

**Figure 4**

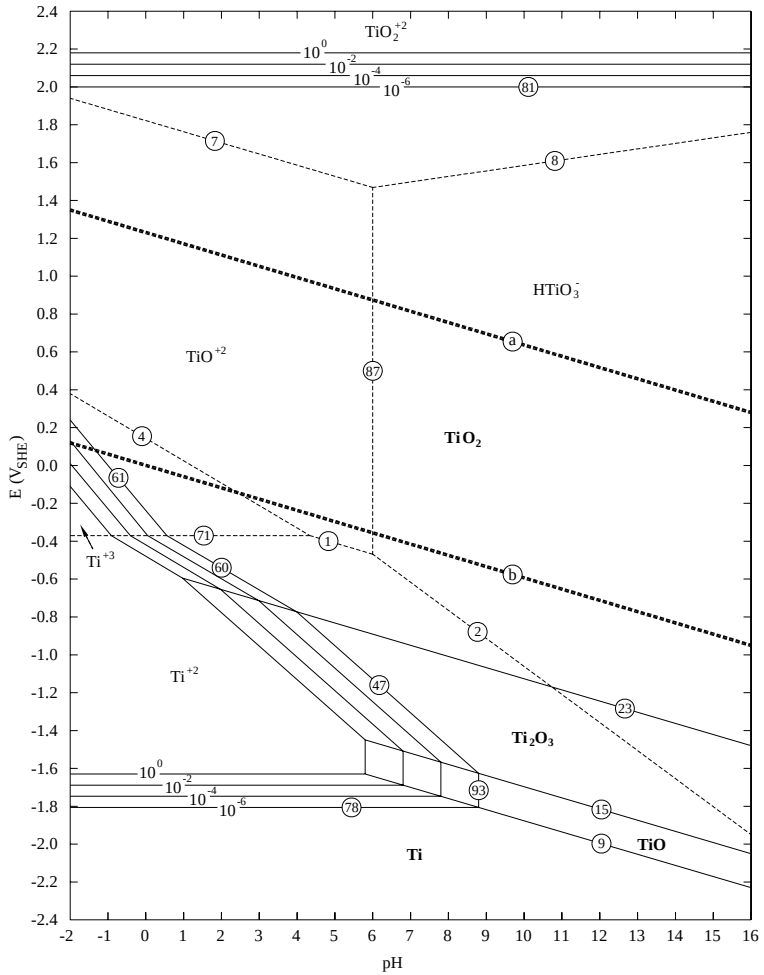
TiO2+2
10 0
10 -2
10 -4
10 -6
HTiO3-
TiO +2
TiO2
Ti +3
Ti +2
Ti2O3
Ti
TiO
E (VSHE)
pH

(a)

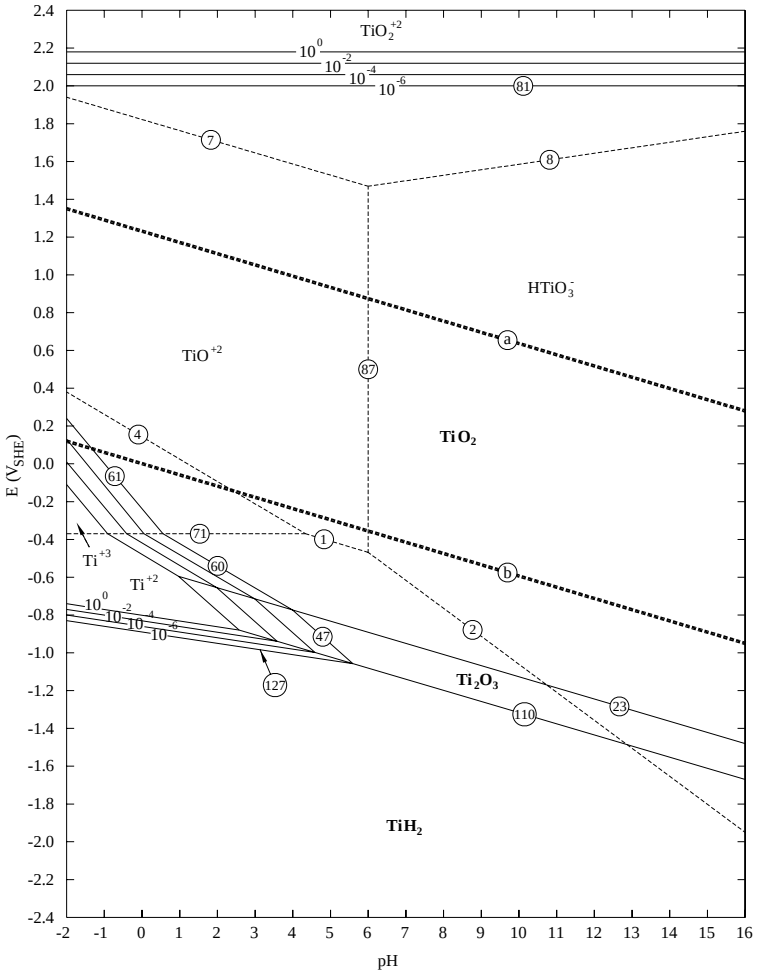
TiO2+2
10 0
10 -2
10 -4
10 -6
HTiO3-
TiO +2
TiO2
Ti +3
Ti +2
Ti2O3
TiH2
E (VSHE)
pH

(b)

**Figure 5**

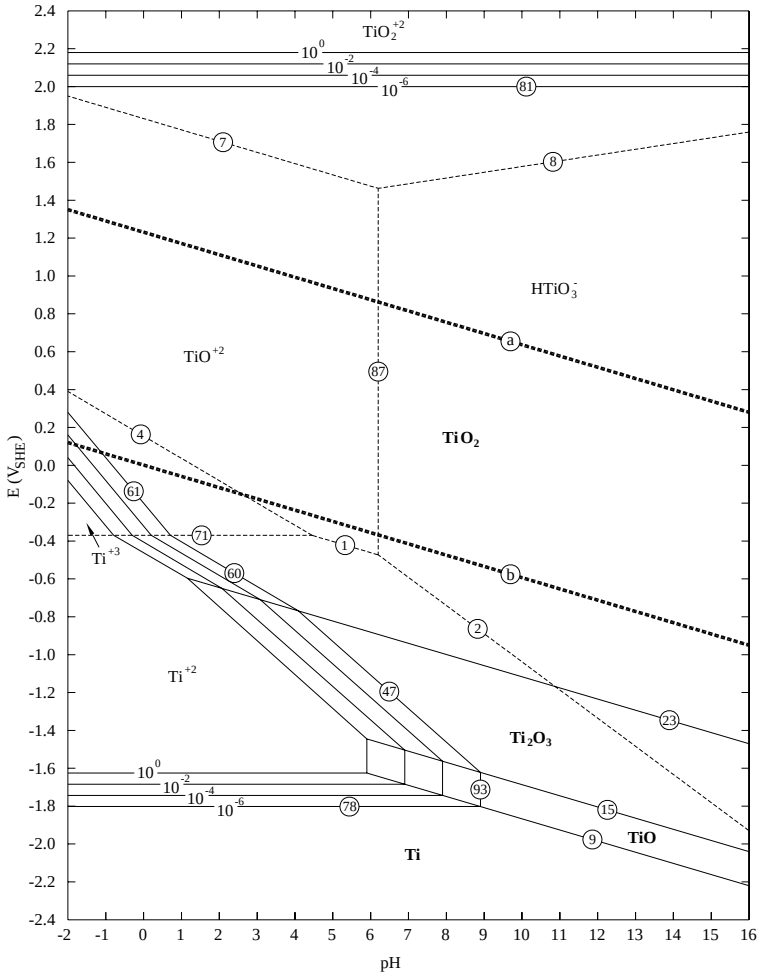
TiO2+2
10 0
10 -2
10 -4
10 -6
81
7
8
HTiO3-
a
TiO+2
87
TiO2
4
61
71
1
Ti+3
60
b
2
Ti+2
47
23
Ti2O3
10 0
10 -2
10 -4
10 -6
93
78
15
9
TiO
Ti
E (VSHE)
pH

(a)

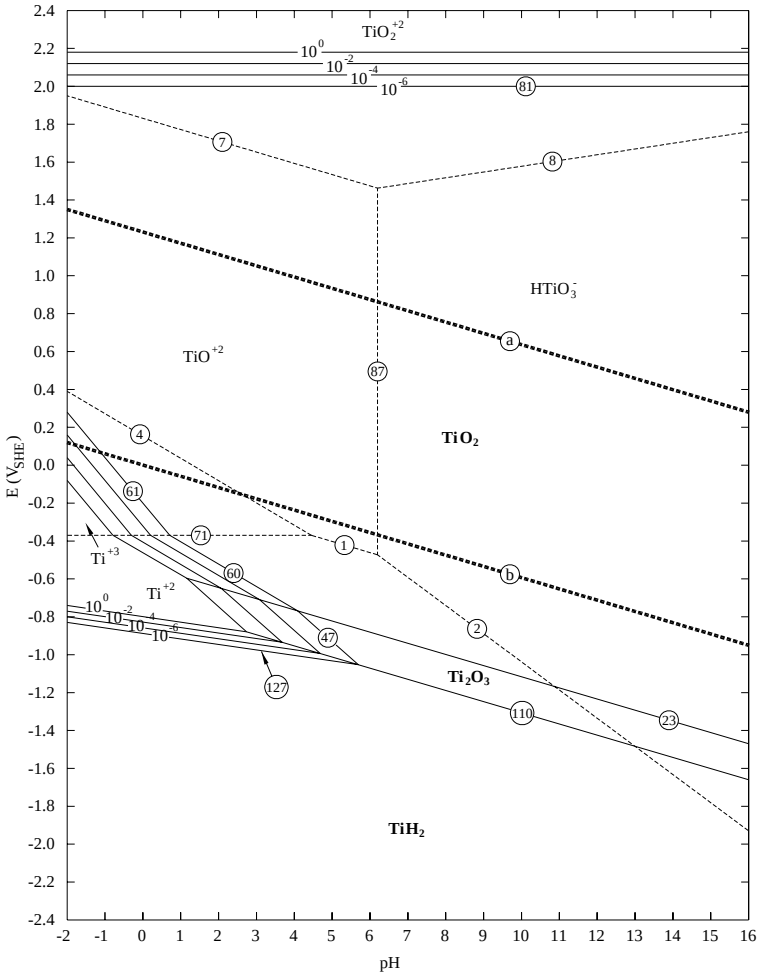
TiO2+2
10 0
10 -2
10 -4
10 -6
81
7
8
HTiO3-
a
TiO+2
87
TiO2
4
61
71
1
Ti+3
60
b
Ti+2
10 0
10 -2
10 -4
10 -6
2
47
127
Ti2O3
110
23
TiH2
E (VSHE)
pH

(b)

**Figure 6**

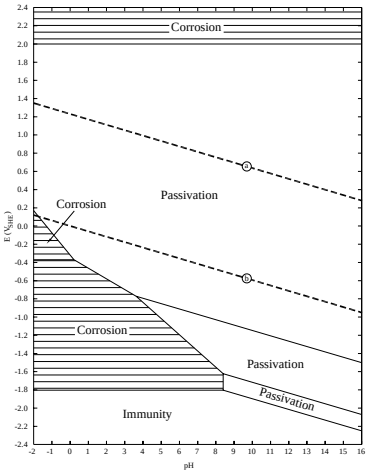


(a)

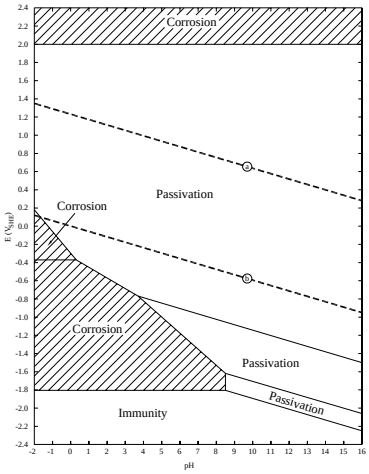


(b)

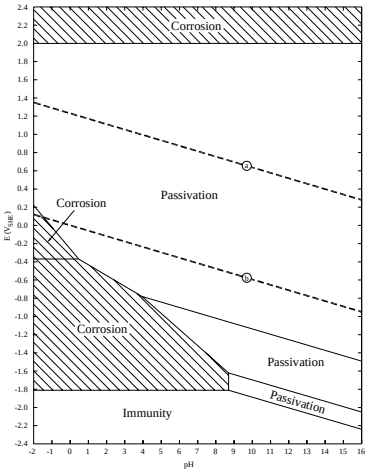


(c)

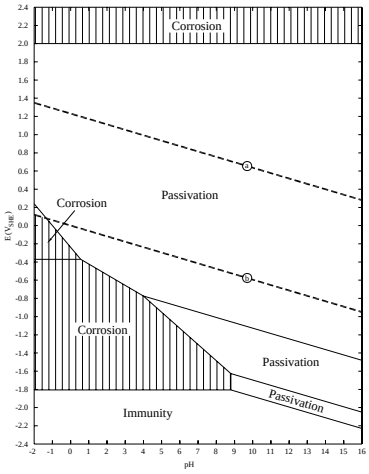


(d)

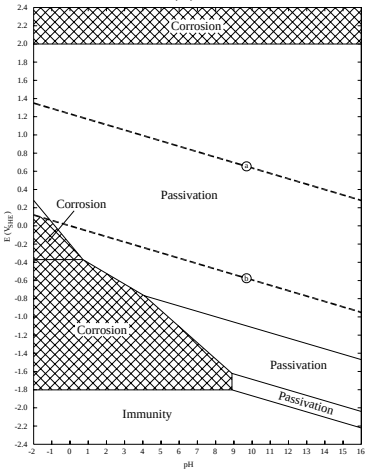


(e)

**Figure 7**

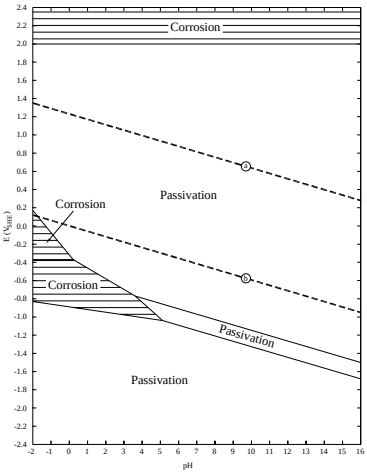


(a)

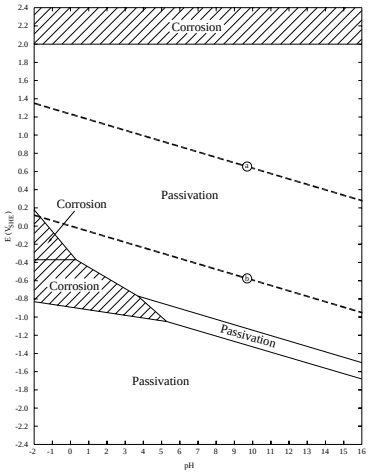


(b)

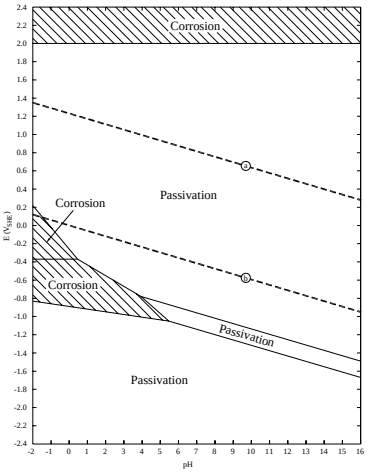


(c)

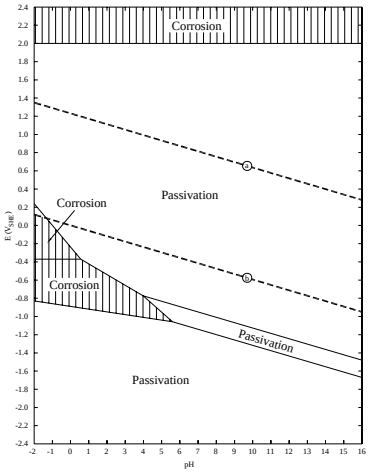


(d)

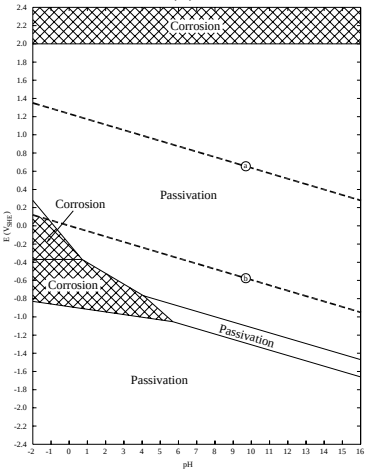


(e)